

Spring 2015

FSAE Electric Vehicle Cooling System Design

Jeff LaMarre

University of Akron Main Campus, jsl29@zips.uakron.edu

Please take a moment to share how this work helps you [through this survey](#). Your feedback will be important as we plan further development of our repository.

Follow this and additional works at: http://ideaexchange.uakron.edu/honors_research_projects



Part of the [Other Mechanical Engineering Commons](#)

Recommended Citation

LaMarre, Jeff, "FSAE Electric Vehicle Cooling System Design" (2015). *Honors Research Projects*. 33.

http://ideaexchange.uakron.edu/honors_research_projects/33

This Honors Research Project is brought to you for free and open access by The Dr. Gary B. and Pamela S. Williams Honors College at IdeaExchange@UAKron, the institutional repository of The University of Akron in Akron, Ohio, USA. It has been accepted for inclusion in Honors Research Projects by an authorized administrator of IdeaExchange@UAKron. For more information, please contact mjon@uakron.edu, uapress@uakron.edu.

FSAE Electric Vehicle Cooling System Design

Jeff LaMarre

Mechanical Engineering – Spring 2015



Contents

Abstract	3
Introduction	4
Theory	5
Radiator Analysis	5
Heat Transfer Analysis	7
Calculations	12
Vehicle Specifications	12
Cooling Load Determination	13
Cooling System Design Overview	17
Radiator Design and Fan Selection	19
Pump Selection	23
Coolant Line Diameter Selection	27
Miscellaneous Design Tasks	29
Motor Coolant Fittings	29
Fan Mounts	31
Duct Design	32
Pump Mount	35
Other Mounting Tabs	35
Manufacturing and Testing	36
Conclusion	37
Acknowledgements	38
Sources	39
Appendix	40

Abstract

The purpose of this project was to design and implement an effective cooling system for the Formula SAE Electric Vehicle. The main components of the drivetrain of the electric vehicle are the motor and the motor controller. The cooling system was designed to cool the motor and motor controller to ensure that they operate in an optimal temperature range thus increasing drivetrain efficiency and ultimately improving vehicle performance.

During the design process, an extensive heat transfer analysis of the water side and air side of a potential radiator was performed. Additionally, system resistance curves and performance curves were calculated, plotted, and utilized in the component selection process. A suitable fan and pump were selected and a radiator was designed.

After determining the critical cooling components, it was necessary to place the components in effective locations within the vehicle. In addition to placing the components, attachment tabs were designed to fix the cooling system to the frame of the vehicle and to fix the fan to the radiator. An inlet duct for the radiator was also created to direct air to the radiator and improve the performance of the system.

Finally, the system was manufactured and assembled on the vehicle. At the time of this report, testing has not yet begun on the vehicle, however, testing will commence shortly and any potential problems or risks will be evaluated and modifications will be performed before the vehicle is entered into competition.

Introduction

Although the 2015 season marks the second year for the FSAE Electric Vehicle Team, it is the first year that the team has designed an entire vehicle from the tires to the roll hoop. The goal for this year's vehicle is to have a simple, reliable, well-built vehicle that can respectably compete at the Formula SAE competition in Lincoln, Nebraska.

The 2015 EV is a dramatic improvement from the previous year's vehicle. The vehicle is designed to be significantly lighter, reliable, and faster than last year's vehicle. Additionally, the operating voltage has been increased from 30 volts to a massive 300 volts.

Not surprisingly, such drastic improvements come with a unique set of challenges for the vehicle as a whole but specifically for the cooling system. With an operating voltage of only 30V, the 2014 EV had no form of cooling system. With no cooling system on the 2014 vehicle, there was no benchmark for the 2015 vehicle. Not only did this mean there was no previous design to improve upon, but there was no cooling performance data of any kind. Additionally, there was no temperature data for the motor or motor controller. Therefore, the cooling system design was initiated with an intensive research phase of racing cooling systems from various circuits and successful FSAE programs' as well as an extensive search for any form of radiator core technical data. As such the design goal for the cooling system was not only to be a simple, effective system, but to become the cooling benchmark for the FSAE Electric Vehicle Team.

Theory

The theory of a cooling system consists of the analysis of the water flow, the analysis of the air, and the analysis of the radiator.

Radiator Analysis

There are various types of automotive heat exchangers but the most common are cross-flow and down-flow radiators. A cross-flow radiator is a radiator in which the fluid tanks are located on the sides of the radiator core; the coolant flows across the core of the radiator from tank to tank. In a down-flow radiator, the tanks are located on the top and bottom of the core and the coolant flows through the core from top to bottom. Cross-flow and down-flow radiators of the same measurements are equally effective at dissipating heat, therefore the decision between cross-flow and down-flow is usually determined by fitment.



Figure 1: An example of a cross-flow radiator [1]



Figure 2: An example of a down-flow radiator [1]

Automotive radiators consist of two end tanks (inlet and outlet), which hold the cooling fluid, and a core. The core of a radiator is comprised of tubes and fins. The tubes run lengthwise from tank to tank and the fins are located in the spaces between the tubes. The fins serve the purpose of increasing the heat transfer area of the radiator without crippling the mass flow rate of air across the radiator. When the radiator is operating, coolant flows through the tubes as airflows through the core of the radiator and across the fins. This airflow across and through the radiator lowers the temperature of the coolant. Therefore, an automotive heat exchanger operates via the principle of cross-flow convection. A diagram of this mechanism is depicted below.

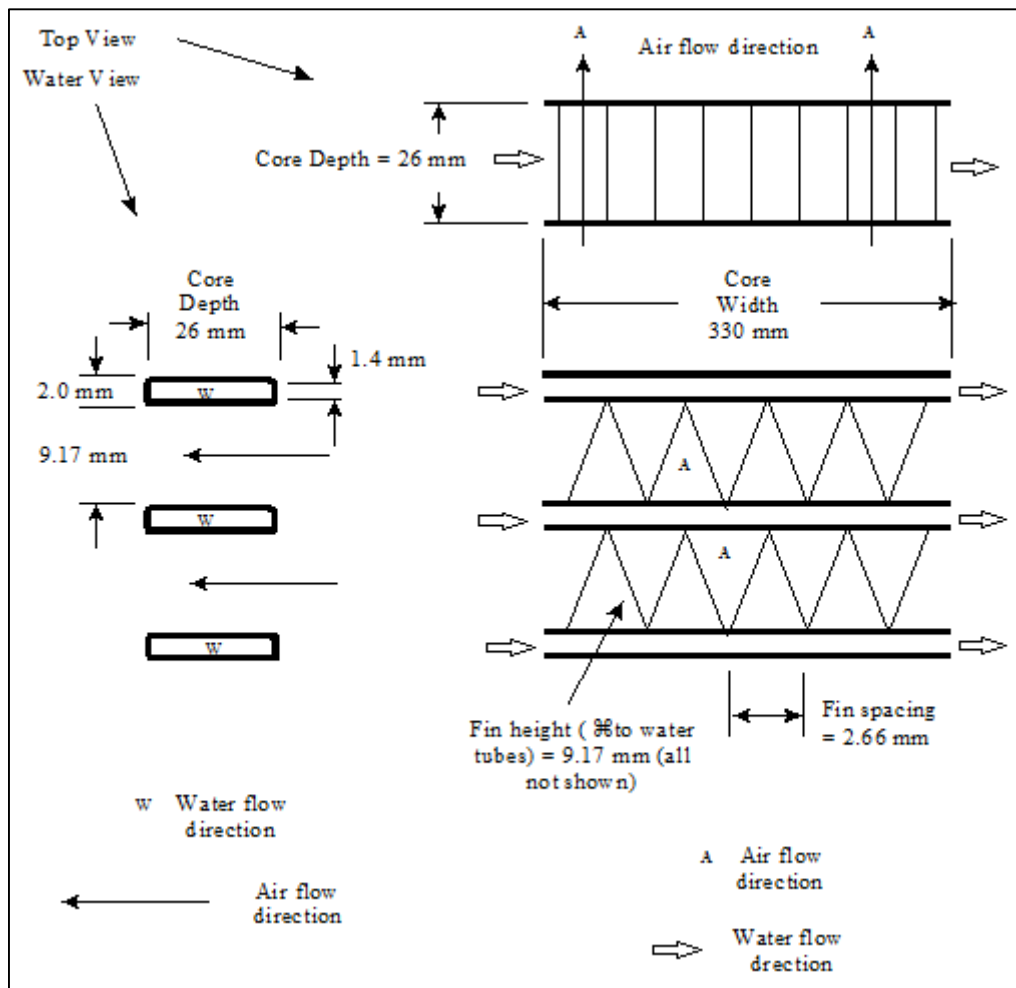


Figure 3: Illustration of an unmixed-unmixed, cross-flow, single-pass radiator [2]

Using this diagram, the area of the tubes, the area of the fins, and other various specifications about airflow and water flow can be determined.

For some applications, it might be necessary to use a radiator with a multi-pass core such as a double-pass or a triple-pass radiator. A double-pass radiator operates like it sounds: the water in the tubes crosses the radiator twice before reaching the outlet. Similarly, in a triple-pass radiator the water passes through the core three times before reaching the outlet. A significant increase in heat dissipation is expected when using a double-pass radiator over a single-pass, however, there is also an increase in the pressure drop of water and therefore a pump that is suitable for a system with a single-pass radiator might not be suitable for the same system with a double-pass radiator.

Heat Transfer Analysis

In an electric vehicle's cooling system, heat is transferred between the drivetrain (motor and motor controller) and the cross-flow radiator. In order for the cooling system to work properly, the rate of heat transferred by the drivetrain must be equal to the rate of heat transferred by the airflow and the water flow. This is shown below:

$$\dot{Q}_{DT} = \dot{Q}_{AIR} = \dot{Q}_W \quad (1)$$

where the subscripts DT, AIR, and W, represent drivetrain, airflow, and water flow, respectively. Note that the rate of heat transfer is lost by the water in the tubes and gained by the air passing through the radiator. If this equation is expanded, the following is obtained:

$$\dot{Q}_{DT} = \dot{m}_{AIR} c_{pAIR} (T_{AIRO} - T_{AIRI}) = \dot{m}_W c_{pW} (T_{WO} - T_{WI}) \quad (2)$$

where \dot{m} is the respective substance's mass flow rate, c_p is the specific heat capacity of the respective substance, T_o is the temperature of the respective substance's outlet temperature, and T_i is the temperature of the respective substance's inlet temperature.

The rate of heat transfer of the cross-flow radiator can be calculated using **Equation 3**, where U_o represents the overall heat transfer coefficient of the radiator, A_o represents the heat transfer surface area of the radiator, F , represents the radiator's correction factor, and $LMTD_{CF}$ represents the log mean temperature difference for a cross-flow heat exchanger. The overall heat transfer coefficient of the radiator and the heat transfer surface area of the radiator are both dependent on the core characteristics of the radiator as well as the characteristics of the airflow and water flow.

$$\dot{Q}_{HX} = U_o A_o F LMTD_{CF} = U_o A_o F \frac{[T_{WI} - T_{AIRO}] - [T_{WO} - T_{AIRI}]}{\ln \left[\frac{T_{WI} - T_{AIRO}}{T_{WO} - T_{AIRI}} \right]} \quad (3)$$

The overall heat transfer coefficient can be calculated using the following equation:

$$U_o = \frac{1}{R_o + R_{wall} + R_i} = \frac{1}{\frac{1}{h_o} + \frac{A_o t_{wall}}{A_i k_{wall}} + \frac{A_o}{A_i h_i}} \quad (4)$$

where R_o , R_{wall} , and R_i represent the heat transfer resistance outside of the water tubes, in the wall of the water tubes, and inside of the water tubes, respectively. Additionally, A_o and A_i are the outside and inside surface areas of the water tubes that are in contact with the water, t_{wall} is the thickness of the tube wall, k_{wall} is the thermal conductivity of the tube material, h_o is the outside (air) convective heat transfer coefficient, and h_i is the internal (water) convective heat transfer coefficient. By analyzing **Equation 4** it can be seen that the heat transfer resistivities can be evaluated as follows.

$$R_o = \frac{1}{h_o} \quad (5)$$

$$R_{wall} = \frac{A_o t_{wall}}{A_i k_{wall}} \quad (6)$$

$$R_i = \frac{A_o}{A_i h_i} \quad (7)$$

Furthermore, the outside convective heat transfer coefficient can be represented by the following equation:

$$h_o = \frac{k_{AIR} \overline{NU}_{AIR}}{D_{hAIR}} \quad (8)$$

where k_{AIR} is the thermal conductivity of air, \overline{NU}_{AIR} is the Nusselt number for air flowing through the air channels, and D_{hAIR} is the hydraulic diameter of the air channel between the water tubes and fins. The hydraulic diameter and the Nusselt number of the air channels can be calculated using **Equation 9** and **Equation 10**, respectively.

$$D_{hAIR} = \frac{4(\text{Air Flow Area})}{\text{Air Flow Perimeter}} = \frac{4(0.5 \text{ Fin Height})(\text{Fin Spacing})}{(\text{Fin Spacing}) + 2(\text{Fin Height})} \quad (9)$$

$$\overline{NU}_{AIR} = 1.86 \left(\frac{Re_{air} Pr_{air}}{\frac{L_{air}}{D_{hAIR}}} \right)^{\frac{1}{3}} \quad (10)$$

Note that Re_{air} is the Reynolds number of the airflow, Pr_{air} is the Prandtl number of the airflow, and L_{air} is the fin length. The Reynolds number of the airflow can be evaluated as the following:

$$Re_{air} = \frac{V_2 D_{hAIR}}{\nu_{air}} \quad (11)$$

where ν_{air} is the kinematic viscosity of the air, and the increase in air velocity through the channel, V_2 , can be evaluated as

$$V_2 = V_1 \frac{A_{air1}}{A_{air2}} = V_1 \frac{\text{Surface Area of Radiator Face}}{A_{air1} - (\text{Frontal Area of Tubes}) - (\text{Frontal Area of Fins})} \quad (12)$$

where V_1 is the approach air velocity. After determining these variables, one is able to use **Equation 3** and **Equation 4** to determine the necessary overall heat transfer coefficient of the radiator for the required rate of heat transfer.

Quite a few conclusions can be reached by analyzing the airflow rate of the cooling system. Realizing that the a radiator consists of three different resistances to the heat transfer from water to air, it can be observed that the thermal resistance of air is greater than the thermal resistance of the water and the thermal resistance of the tube wall and fins. Thus, it is necessary to determine the required airflow through the radiator and select a combination of radiator and cooling fan which is capable of producing this airflow. **Figure 4** depicts the profile view of the radiator and fan orientation. Note that the airflow reaches the radiator before the fan meaning the fan is in a pulling configuration.

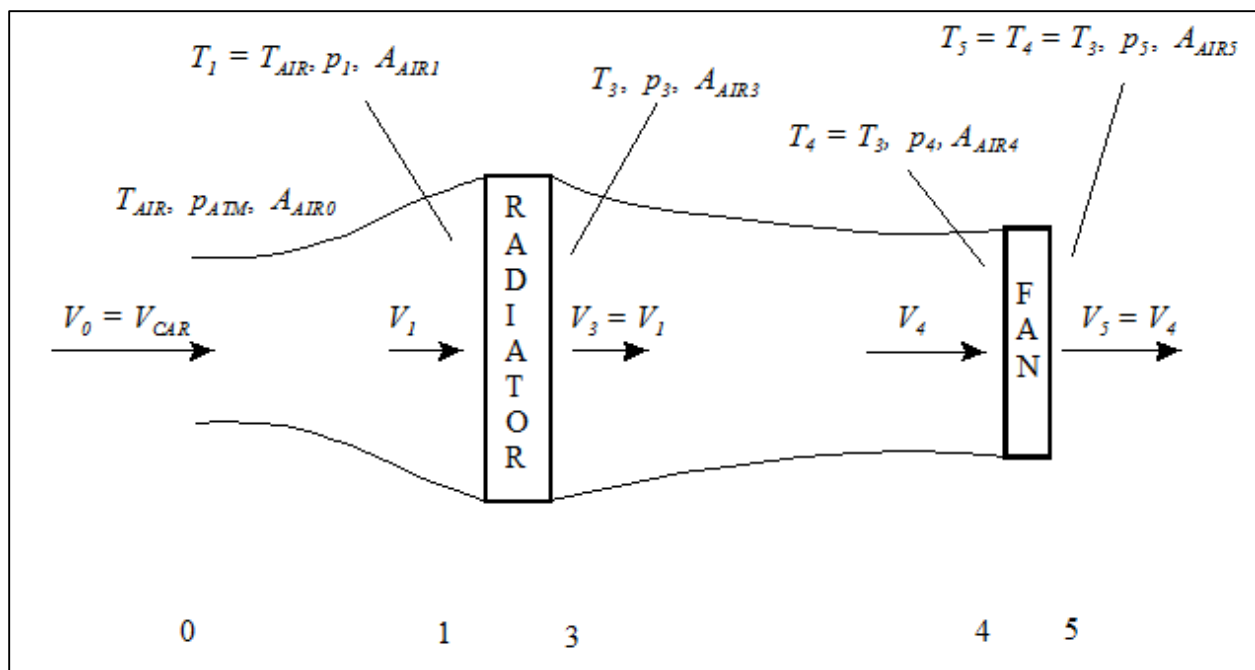


Figure 4: Airflow model through radiator and cooling fan [2]

If Bernoulli's equation is written for point 0 to point 1 in **Figure 4**, the following is obtained.

$$\frac{P_{ATM}}{\rho_{AIR}} + \frac{V_{car}^2}{2} = \frac{P_1}{\rho_{AIR}} + \frac{V_1^2}{2} \quad (13)$$

If the mechanical energy equation is used to analyze the flow through the radiator (point 1 to point 3), the following is obtained:

$$P_1 - P_3 = K_R \rho_{AIR} \frac{V_1^2}{2} \quad (14)$$

where K_R is the loss coefficient due to pressure loss across the radiator. Continuing with this approach, Bernoulli's equation from point 3 to point 4 yields **Equation 15**.

$$\frac{P_3}{\rho_{AIR}} + \frac{V_3^2}{2} = \frac{P_4}{\rho_{AIR}} + \frac{V_4^2}{2} \quad (15)$$

The static pressure rise of the cooling fan can be represented as a function of the airflow rate as follows:

$$P_5 - P_4 = C_o - C_1 Q_F - C_2 Q_F^2 \quad (16)$$

where Q_F is the volumetric flow rate of air passing through the fan and C_o , C_1 , and C_2 are constants for a quadratic representation of the fan static pressure rise. If this relationship is assumed to be linear, C_2 is equal to zero, and **Equation 17** is obtained.

$$P_5 - P_4 = C_o - C_1 Q_F \quad (17)$$

where C_o is the intercept of the linear regression and C_1 is the slope of the linear regression. The pressure difference between point 0 and point 4 can be represented as follows:

$$P_0 - P_4 = (P_0 - P_1) + (P_1 - P_3) + (P_3 - P_4) + (P_4 - P_5) = 0 \quad (18)$$

Realizing that P_0 and P_4 are both equal to atmospheric pressure and substituting **Equation 13**, **14**, **15**, and **16** into **Equation 17** yields the following.

$$\frac{\rho_{AIR}}{2} [(V_1^2 - V_{car}^2) + K_R V_1^2 + (V_4^2 - V_3^2)] - (C_o - C_1 Q_F) = 0 \quad (19)$$

The velocity of air at point 1, point 3, and point 4 can be written as **Equations 20**, **21**, and **22**.

$$V_1 = \frac{Q_F}{A_{air1}} \quad V_3 = \frac{Q_F}{A_{air3}} \quad V_4 = \frac{Q_F}{A_{air4}} \quad (20), (21), (22)$$

By analyzing **Figure 4**, it can be seen that the area at point 1 is equal to the area at point 3. Additionally, since the volumetric flow is constant and the density of air is assumed to be constant, **Equation 19** can be rewritten as **Equation 23**.

$$\left[\frac{\rho_{AIR}}{2} \left(\frac{K_R}{A_{air1}^2} + \frac{1}{A_{air4}^2} \right) \right] Q_F^2 + C_1 Q_F - \left(C_o + \frac{\rho_{AIR}}{2} V_{car}^2 \right) = 0 \quad (23)$$

This equation can be used to solve for Q_F based on the area of the radiator, the area of the fan, the car velocity, and the performance characteristics of a specific cooling fan. **Equation 24** shows the equation in this form.

$$Q_F = \frac{-C_1 \pm \sqrt{(C_1)^2 - 4 \left[\frac{\rho_{AIR}}{2} \left(\frac{K_R}{A_{air1}^2} + \frac{1}{A_{air4}^2} \right) \right] \left[- \left(C_o + \frac{\rho_{AIR}}{2} V_{car}^2 \right) \right]}}{\left[\frac{\rho_{AIR}}{2} \left(\frac{K_R}{A_{air1}^2} + \frac{1}{A_{air4}^2} \right) \right]} \quad (24)$$

The volumetric flow rate obtained from this equation can be compared with the volumetric flow rate required by the system. An iterative process can then be used to determine the proper values of the variables within the equation.

Calculations

Vehicle Specifications

In order to simplify the succeeding portions of this document, a small number of drivetrain specifications are listed in the following table.

2015 FSAE EV Drivetrain Overview	
Motor Specifications	
Manufacturer	Enstroj
Model	Emrax 228 HV
Cooling Method	Combined
Min. Water Flow Rate	8 LPM
Min. Inlet Pressure	1.2 bar
Operating Temp.	-30°C - 120°C
Coolant Temp.	40°C
Motor Efficiency	93% - 98%
Motor Controller Specifications	
Manufacturer	Rinehart Motion Systems
Model	PM100DX
Cooling Method	Water
Flow Rate	8 - 12 LPM
Pressure Drop	0.2 bar
Operating Temp.	-40°C - 80°C
Coolant Temp.	-40°C - 80°C
Controller Efficiency	89% (estimated)
System	
Max Voltage	294 V
Max Current	240 A
Max Power	70.6 kW

Table 1: 2015 FSAE Electric Vehicle Drivetrain Overview

Cooling Load Determination

The first necessary step in the design of the electric vehicle's cooling system was to determine the cooling load produced by the vehicle. The cooling load is the amount of heat that needs to be dissipated by the cooling system.

There are number of methods to roughly estimate the cooling load of the vehicle. The most rudimentary method is to simply assume the overall drivetrain efficiency of the vehicle and further assume that all inefficiencies result in heat generation. For example, assume the vehicle has an overall drivetrain efficiency of 75% and further assume that the 25% inefficiency is given off entirely to heat.

Understanding that the max power of the system is 70.6 kW, the following equation shows the determination of the cooling load for this hypothetical scenario.

$$\dot{Q} = (1 - \eta)P_{max} = (1 - .75)70.6kW = \mathbf{17.7 kW} \quad (25)$$

Clearly using this method is a good way to obtain a simple albeit rough estimate of the cooling load. However, this method should not be used for anything beyond an initial estimate.

A more accurate method of estimating the cooling load of the vehicle is to consider the estimated efficiencies of the motor and motor controller. Referencing **Table 1**, the efficiency of the Enstroj Emrax 228 motor is 93% to 98% and the efficiency of the RMS PM100DX motor controller is 89%. These efficiencies can be used to estimate the cooling load in **Equation 26**.

$$\dot{Q} = (1 - \eta_{mtr})(1 - \eta_{cntrlr})P_{max} = \left(1 - \left(\frac{.93 + .98}{2}\right)(.89)\right)70.6kW = \mathbf{10.6 kW} \quad (26)$$

It is obvious that this estimate is much more accurate than that made in **Equation 25**, however, there are still some issues with this estimate. For one, this is assuming the motor and motor controller are always operating at these generic efficiencies. In reality, the efficiencies of the motor and motor controller are constantly changing based on their respective instantaneous operating points. The efficiency of the motor is dependent upon the instantaneous motor speed and the instantaneous torque output. Similarly, the efficiency of the motor controller is dependent upon the instantaneous operating voltage as well as the instantaneous operating current.

Another issue with this estimate is that there is no consideration for actual power output. For the sake of this estimate, power output is assumed to be constantly at a maximum. This would be an extraordinary occurrence for a typical FSAE race track in which chicanes, hairpins, and other tight technical sections of track abound. In fact, for some tracks it could be said that a vehicle is rarely

operating at full power. The driver’s inputs are dynamic throughout the duration of a race: acceleration out of a turn and along a straight section, deceleration before a turn, constant velocity through the apex of a turn, and perhaps even short segments of the track where the vehicle is coasting with no power input. Therefore it is necessary to consider the power cycle that the vehicle will undergo during a race.

To accurately perform this analysis, *OptimumG’s* vehicle dynamics simulation software *Optimum Lap* was utilized. *Optimum Lap* is a powerful piece of software that drastically reduces the complexity of vehicle dynamics simulation and analysis. Important specifications of the 2015 EV such as tire data, motor curve data, vehicle weight, drive type, and aero data, were first entered into *Optimum Lap*. A sample of this input data is shown in **Figure 5**.

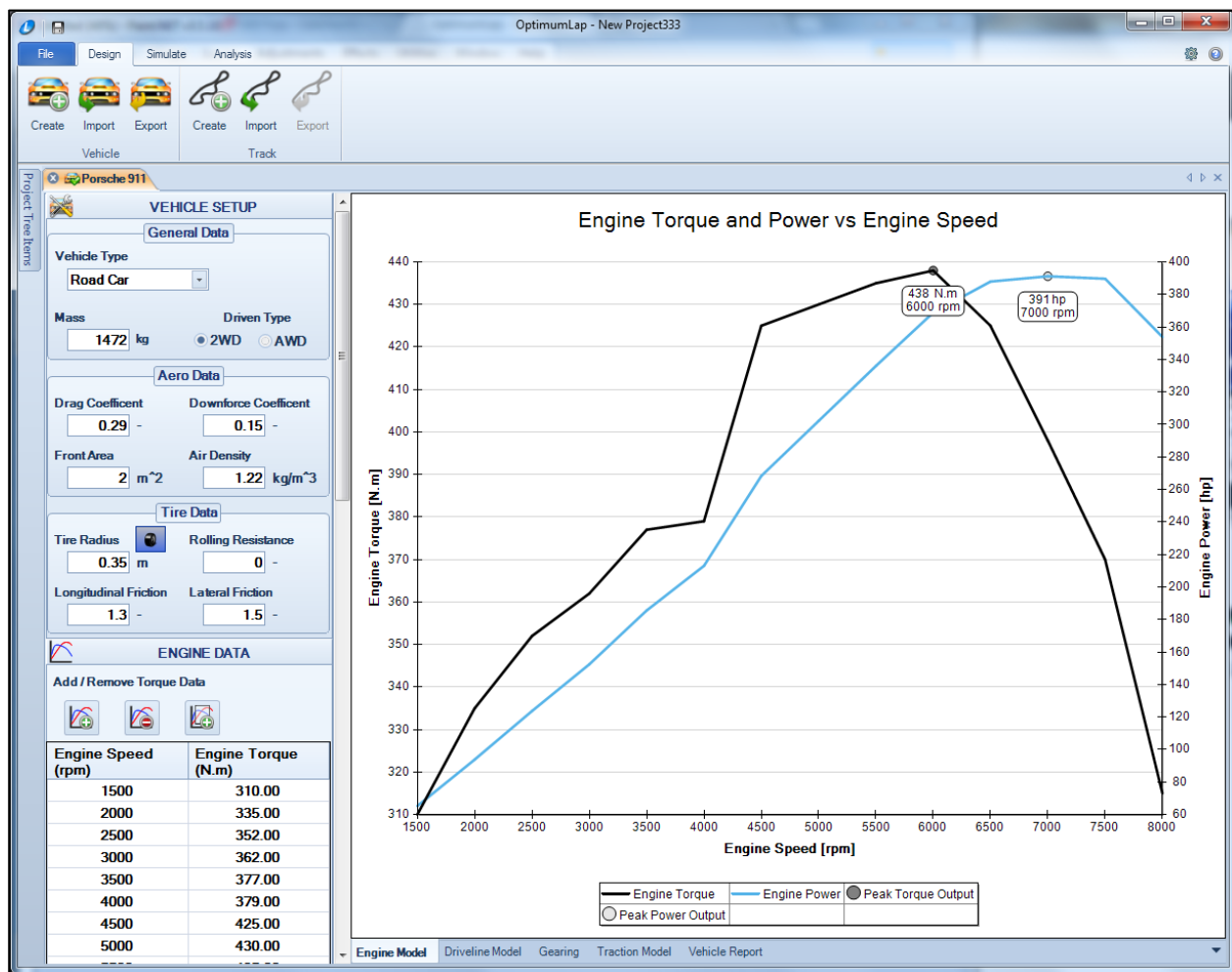


Figure 5: Example vehicle data information input for Optimum Lap vehicle dynamics software [3]

The endurance track from the 2012 Lincoln, Nebraska FSAE competition was then entered into the software. A model of this track, displayed below, was provided by *OptimumG*. The endurance track was chosen over the autocross track because the endurance event is the most demanding of the dynamic events. More heat will be generated by the drivetrain during the endurance event than any other event.



Figure 6: 2012 Lincoln, Nebraska FSAE competition endurance track [4]

Performing the *Optimum Lap* simulation yielded a large amount of data including vehicle velocity, longitudinal and lateral acceleration, elapsed time, motor speed, power output, and other various information. This data was exported into a spreadsheet by 0.010 second increments resulting in over 4600 data points. From this data, the motor current could be determined at any instant of time using the following equation:

$$P = VI \quad (27)$$

where P is power, V is voltage, and I is current. Note that for this calculation, it was assumed that voltage remains constant at 294V while current varies. The heat generated by the motor controller was then calculated using this data and the following equation provided by the motor controller manufacturer, Rinehart Motion Systems.

$$P_{ctrlloss} = (0.00554 * V^{0.85029} * I^C) + 211.5 \quad (28)$$

The heat generated by the motor was then calculated using the efficiency map provided by Enstroj, the motor manufacturer. This efficiency map is displayed in **Figure 7**.

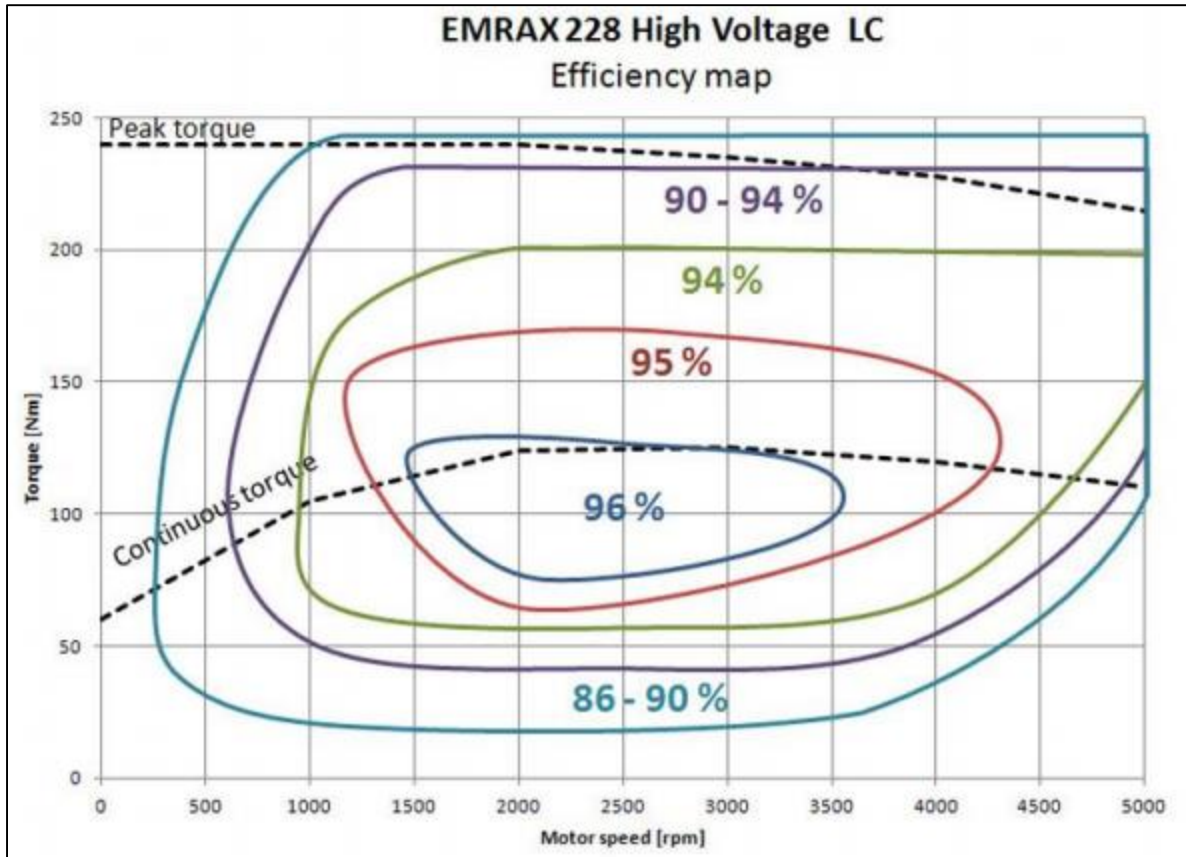


Figure 7: Enstroj Emrax 228 efficiency map [5]

By analyzing **Figure 7**, it becomes apparent that the motor efficiency is a function of motor speed and torque. Using this observation, the colored efficiency areas were quantified and entered into the spreadsheet. “If logic” statements were then used to calculate the instantaneous efficiency of the motor based on the motor torque and motor speed at any given data point. After determining the instantaneous efficiency, the following equation was used to calculate the power lost to heat by the motor at any instant.

$$P_{mtrloss} = (1 - \eta_{inst.})P_{inst.} \quad (29)$$

The heat generated by the motor controller and motor were then summed at all data points.

Considering this heat loss with respect to time and finding an average, the overall cooling load was determined to be **8.2 kW**. After determining this cooling load, the design process was able to move forward to radiator design and fan selection.

Cooling System Design Overview

The cooling system must cool two things: the motor and the motor controller, which are both liquid cooled. As mentioned before, a cross-flow radiator is required to properly cool the drivetrain. Since it was determined that the motor generates more heat than the motor and it requires a lower coolant inlet temperature, the motor was placed at the beginning of the cooling circuit. Therefore, it was determined that the cooling circuit would consist of an electric water pump, the motor, the motor controller, and finally the radiator. This circuit and orientation is depicted in the schematic in **Figure 8**.

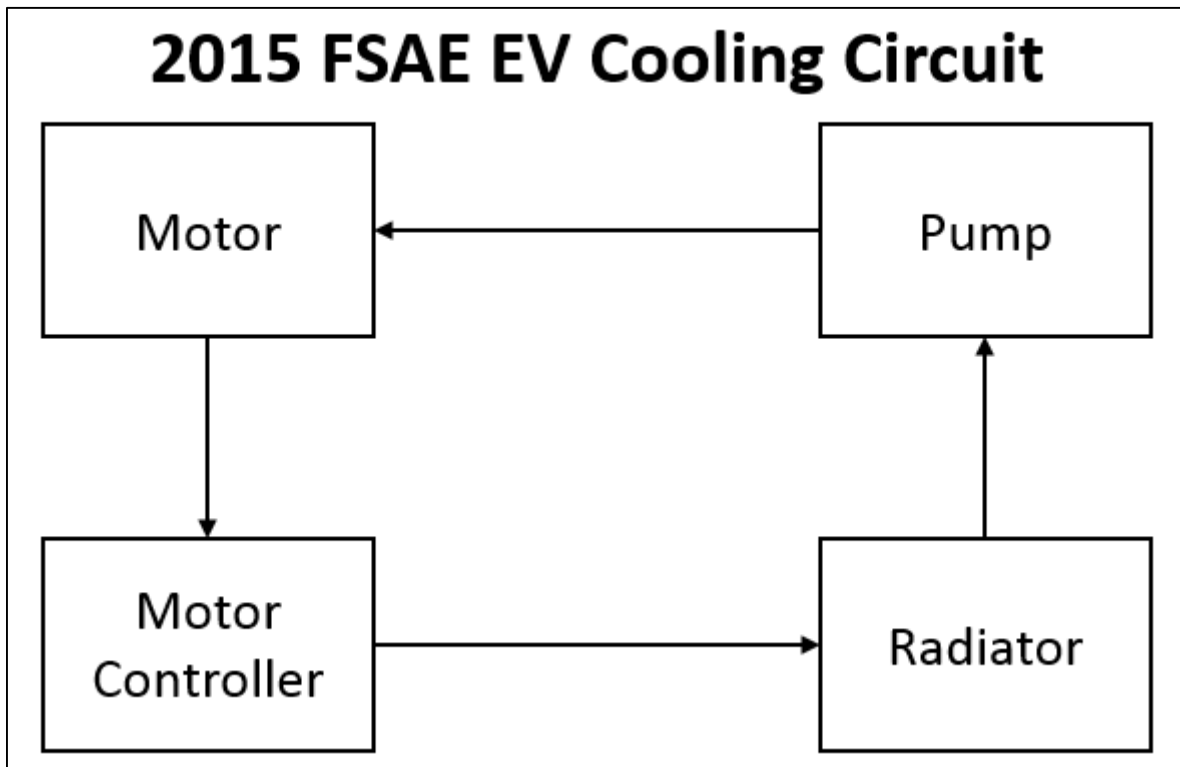


Figure 8: Cooling circuit schematic

By analyzing a potential radiator, it was decided that the inlet and outlet temperatures of water as well as the inlet air temperature could be determined. The inlet air temperature was determined to be **25°C** by analyzing historical weather data for the week of June 18 (date of 2015 competition) at the Lincoln, Nebraska Airport. Knowing that the first component being cooled is the motor, the outlet water temperature was determined to be **40°C** based on the stipulation that the inlet temperature of the water entering the motor must be 40°C. The inlet water temperature was determined by rearranging **Equation 2** as shown in **Equation 30**.

$$T_{WI} = T_{WO} - \frac{\dot{Q}}{\dot{m}_W c_{pW}} = 40^\circ\text{C} - \frac{8.2\text{kW}}{\left(\frac{12\text{ L}}{60\text{ s}}\right) \left(\frac{1\text{ kg}}{\text{L}}\right) \left(4.2 \frac{\text{kJ}}{\text{kg}^\circ\text{C}}\right)} = 30.2^\circ\text{C} \quad (30)$$

Note that \dot{m}_W is the mass flow rate of water and c_{pW} is the specific heat of water. This calculation was performed using a volumetric flow rate of 12 LPM, which is the maximum flow rate permitted by the motor controller. **Figure 9** depicts the water-side and air-side of the radiator.

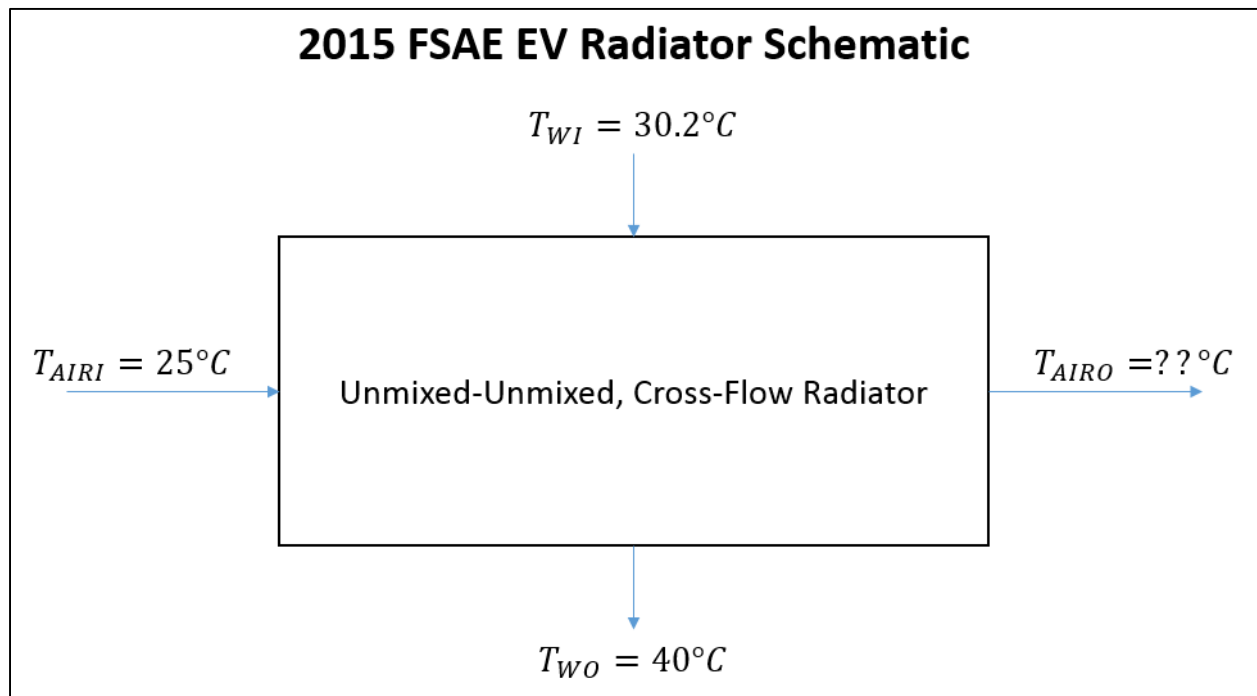


Figure 9: Radiator water-side and air-side schematic

After obtaining these temperature values, the design process can move forward with one of two possible approaches. The first approach is to select a radiator and fan and subsequently calculate the exit air temperature. This process will be iterated until a fan and radiator combination that yields a suitable exit air temperature is obtained. The other method is to fix the exit air temperature to a selected value and select a combination of radiator and fan that yields this exact value.

In order for the radiator to work properly, the exit air temperature should be slightly lower than the exit water temperature. Therefore, 38°C was selected as the target exit air temperature for the radiator. Radiator and fan combinations were selected and numerically tested until the best possible combination was determined. This process is outlined in the **Radiator Design and Fan Selection** portion of this document.

Radiator Design and Fan Selection

Being the first year for a cooling system on the FSAE electric vehicle, there was no current technical radiator data available during the design process. Therefore, it was necessary to work “backwards” from the radiator’s exit air temperature as described in the radiator analysis in the preceding portion of this document. It should be noted that due to the geometry of the vehicle, the radiator size was limited to a height of 11 inches and a width of 16 inches.

Radiator performance data from OEM radiator manufacturer *Visteon* was assumed to be a reasonably accurate reference and was utilized for these calculations. This data, displayed in **Table 2** provides rate of heat dissipation, water side pressure drop, and air side pressure drop based on core length, core height, core depth, and fin density of a single-pass radiator. **Table 3** provides similar data for a double-pass design. Note that this information is accurate for an inlet air temperature of 40°C, an inlet water temperature of 100°C, and a coolant flow rate of 20 LPM.

Core Dimensions and Predicted Performance for Single-Pass Visteon Radiators										
No.	L (mm)	H (mm)	D (mm)	FPDM (Fins/dm)	Face Velocity = $V_1 = 3$ m/s			Face Velocity = $V_1 = 6$ m/s		
					\dot{Q} (kW)	Δp_{AIR} (Pa)	Δp_W (kPa)	\dot{Q} (kW)	Δp_{AIR} (Pa)	Δp_W (kPa)
1	267	210	26	75	8.04	83	3.7	12.61	250	3.7
2	267	232	26	75	8.78	83	3.5	13.63	250	3.5
3	267	255	26	75	9.48	83	3.3	14.58	250	3.3
4	330	255	26	75	11.71	84	3.5	17.73	250	3.5
5	330	277	26	75	12.52	84	3.3	18.73	250	3.3
6	330	300	26	75	13.29	84	3.2	19.63	250	3.2
7	267	237	36	75	10.48	122	1.8	16.27	335	1.8
8	267	259	36	75	11.24	122	1.6	17.15	335	1.6
9	237	280	36	63	11.41	96	1.4	16.48	267	1.4
10	237	302	36	63	12.01	96	1.2	17.12	267	1.2
11	330	204	36	75	11.51	124	2.7	17.94	339	2.7
12	330	226	36	63	11.92	98	2.3	17.54	270	2.3
13	330	248	36	63	12.81	98	2	18.57	270	2
14	330	270	36	63	13.63	98	1.7	19.45	270	1.7

Table 2: Core dimensions and predicted performance for single-pass Visteon radiators [2]

Core Dimensions and Predicted Performance for Double-Pass Visteon Radiators										
No.	L (mm)	H (mm)	D (mm)	FPDM (Fins/dm)	Face Velocity = $V_f = 3$ m/s			Face Velocity = $V_f = 6$ m/s		
					\dot{Q} (kW)	Δp_{AIR} (Pa)	Δp_W (kPa)	\dot{Q} (kW)	Δp_{AIR} (Pa)	Δp_W (kPa)
1	267	210	26	75	8.24	83	10.9	13.39	250	10.9
2	267	232	26	75	9.08	83	9.4	14.5	250	9.4
3	267	255	26	75	9.91	83	8.3	15.74	250	8.3
4	330	255	26	75	12.27	84	9.5	19.22	252	9.5
5	330	277	26	75	13.24	84	8.5	20.61	251	8.5
6	330	300	26	75	14.19	84	7.6	21.93	251	7.7
7	267	237	36	75	10.98	122	10.4	17.9	338	10.5
8	267	259	36	75	11.91	123	8.9	19.24	338	8.9
9	237	280	36	63	12.25	97	7.7	18.72	270	7.7
10	237	302	36	63	13.09	97	6.7	19.85	270	6.7
11	330	204	36	75	11.93	125	16.6	19.33	342	16.6
12	330	226	36	63	12.49	98	13.7	19.11	272	13.8
13	330	248	36	63	13.57	98	11.6	20.6	272	11.6
14	330	270	36	63	14.63	98	10	22.01	271	10

Table 3: Core dimensions and predicted performance for double-pass Visteon radiators [2]

Since the frame geometry of the vehicle limits the radiator to a height of 11 inches, the largest possible fan with the best performance curve was selected. This fan, the SPAL VA15-BP70/LL-39A is a 24V cooling fan that can operate in a push or pull configuration and has a maximum airflow rate of 1174 CFM [6].

Furthermore, it has a blade diameter of 10 inches and a maximum shroud diameter of 11 inches meaning that it is the largest possible fan for a radiator with a height of 11 inches. Using pressure and airflow data provided by SPAL, the performance curve was plotted. This plot is displayed in **Figure 10**. A linear regression was fitted to the performance data and the following regression equation was obtained:

$$P = -755.1(Q_{air}) + 417.37 \quad (31)$$

where the static pressure, P , is in pascals and the volumetric flow rate of air, Q_{air} , is in cubic meters per second. This equation yielded both fan coefficients required in **Equation 24**.

$$C_o = 417.37 \text{ (Pa)} \quad (32)$$

$$C_1 = 755.1 \left(\frac{Ns}{m^5} \right) \quad (33)$$

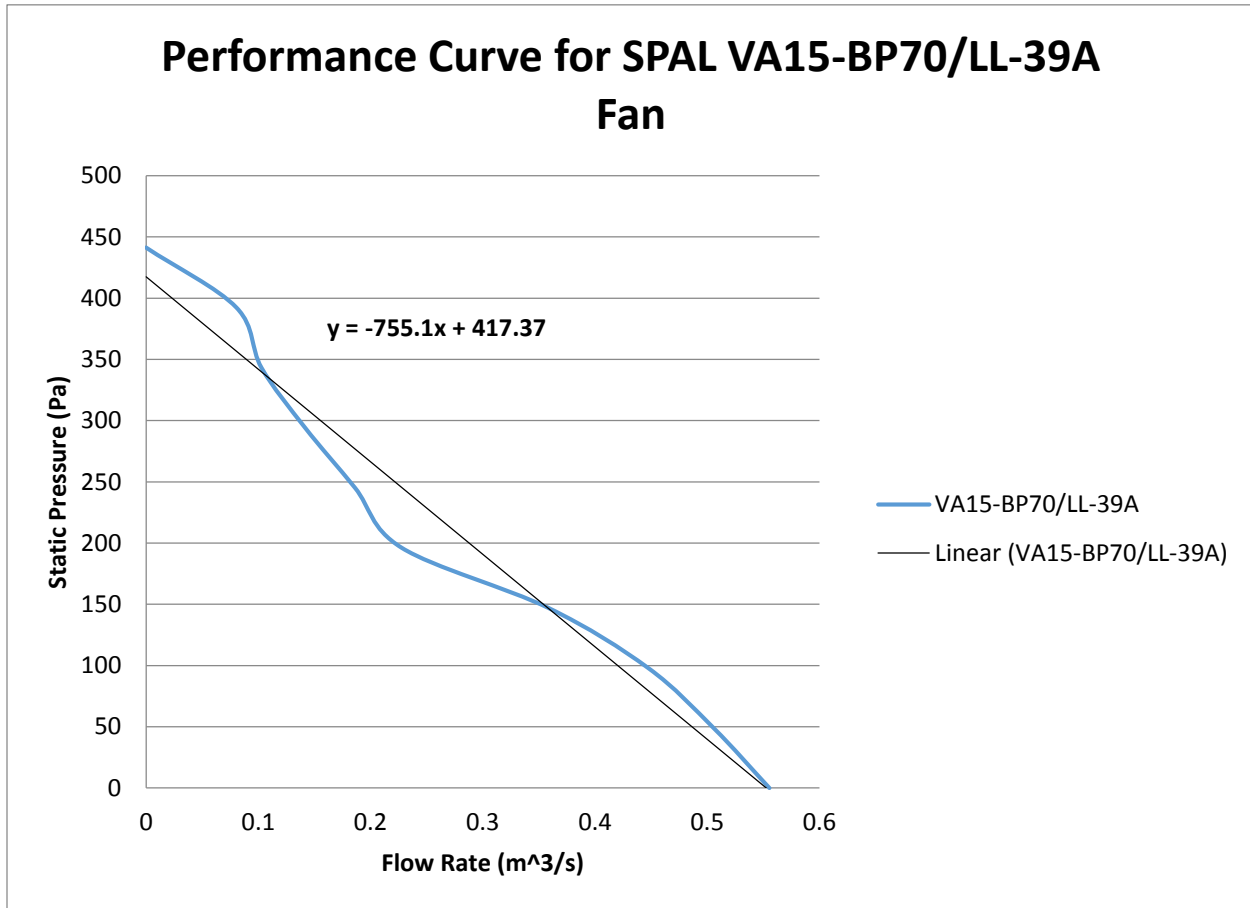


Figure 10: SPAL VA15-BP70/LL-39A fan performance curve

The area of the fan, A_{air4} , required in **Equation 24** was calculated as shown below:

$$A_{air4} = \frac{\pi}{4} d^2 = \frac{\pi}{4} \left[(255 \text{ mm}) \left(\frac{1 \text{ m}}{1000 \text{ mm}} \right) \right]^2 = 0.0511 \text{ m}^2 \quad (34)$$

where d is the fan diameter (10 in or 255 mm).

Two more values were required to solve for the volumetric flow rate of air through the radiator: the radiator loss coefficient, K_R , and the surface area of the radiator core, A_{air1} .

The radiator loss coefficient was calculated using the following equation:

$$K_R = \frac{2\Delta P_{AIR}}{\rho V^2} \text{ (unitless)} \quad (35)$$

where ρ is the density of air, ΔP_{AIR} is the pressure drop of air across the radiator, and V is the face velocity of air across the radiator. The pressure drop data from **Table 2** was used for all Visteon core dimensions at a face velocity of 3 m/s as well as 6 m/s. The average loss coefficient value for all core sizes and both face velocities was determined to be **15.79**.

In order to determine the area of the radiator core, it was necessary to determine the appropriate size of the core of the radiator. Various core areas were tested using **Equation 24**, the average radiator loss coefficient, and the obtained fan data. This process was iterated until a suitable core area was obtained: 0.122 square meters. Due to the size constraints stipulated by the dimensions of the vehicle, this area was not feasible. Unfortunately, as with many engineering tasks, it was not a possibility to use the optimal radiator design due to size limitations. Therefore, it was necessary to maximize the core dimensions of the radiator without crippling the system's ability to dissipate heat. This was an iterative process with the selected radiator supplier, *C&R Racing*. *C&R Racing* was selected due to their superior core manufacturing as well as their historical success with FSAE applications. The smallest header lengths available were 13.75 inches or 17.00 inches. Obviously since the maximum radiator width was 16 inches, the core width became 13.75 inches. This core width coupled with the narrowest tanks (1 inch wide) resulted in an overall radiator width of 15.75 inches. The largest stack height shorter than 11 inches was 10 inches and consequently the finalized core dimensions became 13.75 inches by 10.00 inches by 1.50 inches, and a surface area of 0.89 square meters. Since the system's flow rate is as moderate 12 LPM, a double-pass radiator was selected to increase the radiator's ability to transfer heat. The radiator is displayed in **Figure 11**. The radiator drawing is available in the **Appendix**.

Using the finalized core dimensions, the flow rate was determined using **Equation 24**. The resulting flow rate was **0.400** cubic meters per second. The temperature rise was then determined by rearranging **Equation 2**.

$$\Delta T_{air} = \frac{\dot{Q}}{m_{AIR} c_{Pair}} = \frac{\dot{Q}}{Q \rho c_{Pair}} = \frac{8.2 \text{ kW}}{\left(0.400 \frac{\text{m}^3}{\text{s}}\right) \left(1.165 \frac{\text{kg}}{\text{m}^3}\right) \left(1.00 \frac{\text{kJ}}{\text{kg}^\circ\text{C}}\right)} = 17.6^\circ\text{C} \quad (36)$$

With an air temperature rise of 17.6°C, the radiator will operate optimally in ambient temperatures of 20°C to 22.4°C as opposed to 25°C. Clearly this is not optimal, however, the estimated surface area of the radiator did not include the surface area of the fins, which will decrease the increase in air temperature. Furthermore, these calculations do not include the cooling effects of ambient air. It is believed that the average electric motor is cooled 25% by ambient air. **Equation 37** depicts this change.

$$\Delta T_{air} = \frac{8.2 \text{ kW}(1 - .25)}{\left(0.400 \frac{\text{m}^3}{\text{s}}\right)\left(1.165 \frac{\text{kg}}{\text{m}^3}\right)\left(1.00 \frac{\text{kJ}}{\text{kg}^\circ\text{C}}\right)} = 13.2^\circ\text{C} \quad (37)$$

With an air temperature rise of 13.2°C, the radiator will operate optimally in ambient temperatures of 24.8°C to 26.8°C.

Due to the uncertainty in these assumptions, the real performance of the radiator will not be known until the system undergoes strenuous testing.

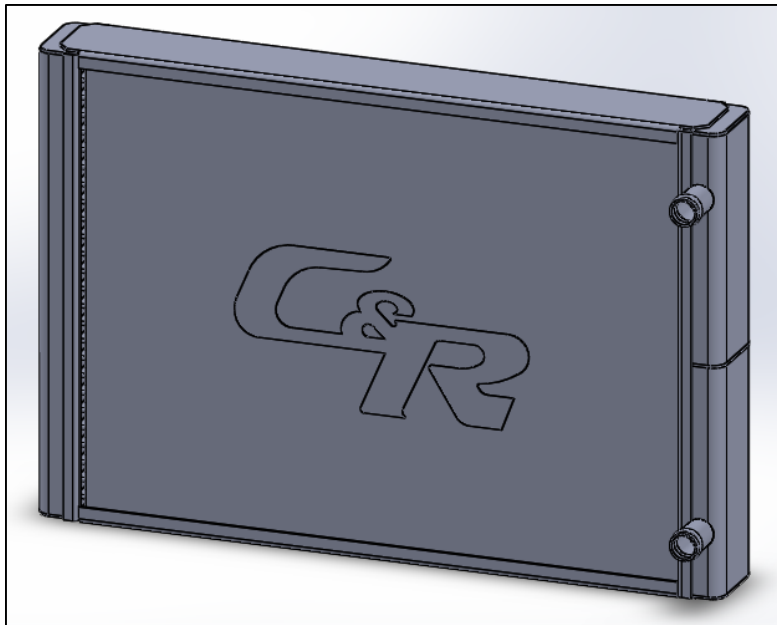


Figure 11: C&R Racing radiator model

Pump Selection

To determine a pump, it was first necessary to determine the system's required water flow rate and pressure. In order to maximize heat transfer, the maximum permitted flow rate was selected.

Determining the required flow rate was as simple as observing the specifications of the motor and motor controller. The maximum flow rate permitted (recommended by manufacturer) by the motor controller was smaller than the maximum flow rate permitted by the motor. Therefore, the maximum flow rate permitted by the motor controller, **12 LPM**, was selected as the flow rate of the system.

To determine the pressure required, it was necessary to determine the pressure drop due to each component as well as the pressure loss through the coolant lines of the system.

To determine the pressure drop due to the components of the system, the following equation was used:

$$\Delta P = kQ_w^2 \tag{38}$$

where ΔP is the pressure drop across a component, Q_w is the flow rate through a component, and k is the loss coefficient of a component. Moreover, the total pressure drop across the system can be written as the following:

$$\Delta P = (k_{MTR} + k_{MC} + k_{HX})Q_w^2 \tag{39}$$

where k_{MTR} is the loss coefficient for the motor, k_{MC} is the loss coefficient for the motor controller, and k_{HX} is the loss coefficient for the radiator.

To determine the loss coefficient of the motor manufacturer inlet pressure data, shown in **Figure 12**, was utilized.

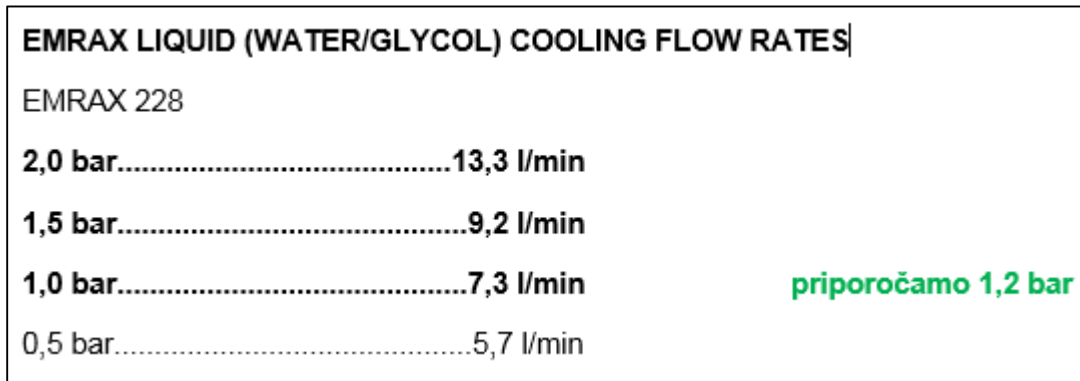


Figure 12: Enstroj Emrax 228 inlet pressure information [7]

The pressures provided are absolute pressures. The inlet pressure for a flow rate of 12 LPM was found via interpolation and was used to solve for the pressure drop across the motor, assuming the exit pressure is atmospheric (1 bar).

$$\Delta P_M = \left[1.5 \text{ bar} + \frac{2 \text{ bar} - 1.5 \text{ bar}}{13.3 \text{ LPM} - 9.2 \text{ LPM}} (12 \text{ LPM} - 9.2 \text{ LPM}) \right] - 1 \text{ bar} = \mathbf{0.84 \text{ bar}} \tag{40}$$

Using this pressure drop, the loss coefficient of the motor was calculated as follows.

$$k_{MTR} = \frac{\Delta P_M}{Q_w^2} = \frac{(0.84 \text{ bar}) \left(\frac{100 \text{ kPa}}{1 \text{ bar}} \right)}{\left[(12 \text{ LPM}) \left(\frac{1 \text{ L}}{1000 \text{ m}^3} \right) \left(\frac{1 \text{ min}}{60 \text{ s}} \right) \right]^2} = \mathbf{2.1 \times 10^9 \frac{\text{kPa s}^2}{\text{m}^6}} \tag{41}$$

A similar process was used to determine the loss coefficient for the motor controller. A plot of pressure drop versus flow rate was provided by the motor controller manufacturer. This data is displayed in **Figure 13**.

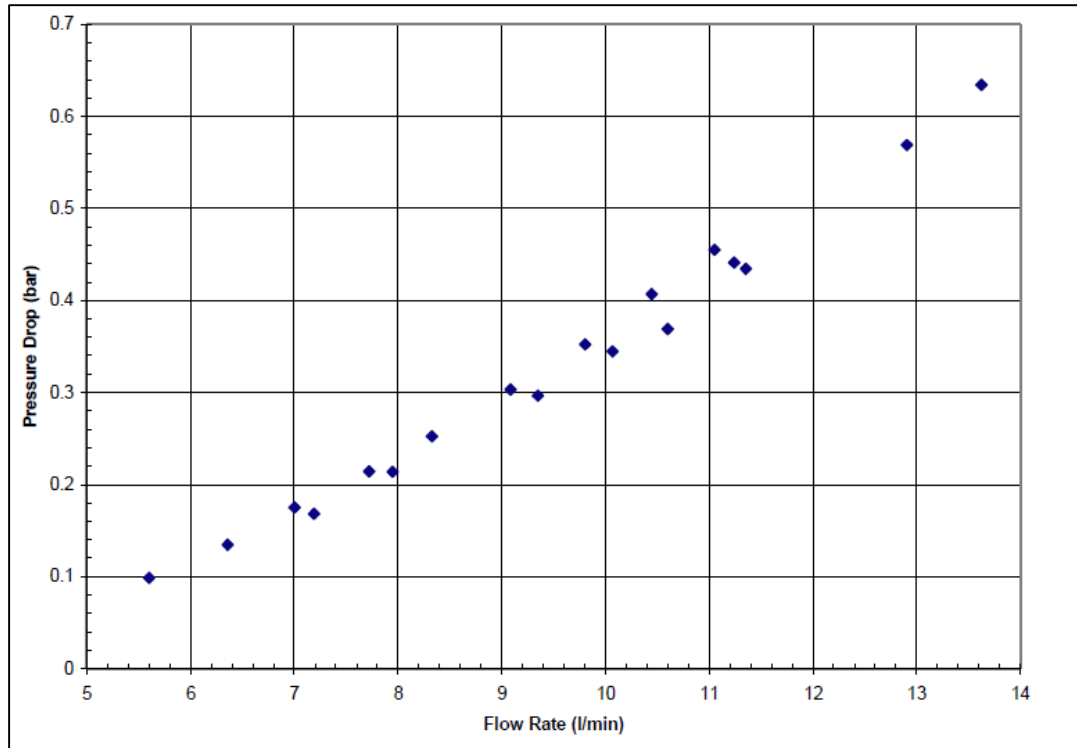


Figure 13: Rinehart Motion Systems PM100DX motor controller pressure drop information [8]

This plot was used to interpolate for the pressure drop at a flow rate of 12 LPM, shown below.

$$\Delta P_{MC} = \left[0.35 \text{ bar} + \frac{0.56 \text{ bar} - 0.35 \text{ bar}}{12.91 \text{ LPM} - 10.00 \text{ LPM}} (12 \text{ LPM} - 10 \text{ LPM}) \right] = \mathbf{0.494 \text{ bar}} \quad (42)$$

Using this pressure drop, the loss coefficient of the motor controller was calculated as follows.

$$k_{MC} = \frac{\Delta P_{MC}}{Q_w^2} = \frac{(0.494 \text{ bar}) \left(\frac{100 \text{ kPa}}{1 \text{ bar}} \right)}{\left[(12 \text{ LPM}) \left(\frac{1 \text{ L}}{1000 \text{ m}^3} \right) \left(\frac{1 \text{ min}}{60 \text{ s}} \right) \right]^2} = \mathbf{1.235 \times 10^9 \frac{\text{kPa s}^2}{\text{m}^6}} \quad (43)$$

To determine the pressure drop in the radiator, the water pressure drop information from **Table 3** was used. Radiator number 14 was selected for this purpose as its core surface area is 89,100 square millimeters. This is reasonably close to the actual radiator's core surface area of 88,710 square millimeters. Additionally, the thicknesses of the radiator cores are approximately the same and the tube lengths are relatively similar (12.9 inches versus 13.75 inches). The pressure drop for this radiator is 10 kPa. Therefore, the loss coefficient of the radiator was calculated as follows.

$$k_{HX} = \frac{\Delta P_{HX}}{Q_w^2} = \frac{(10 \text{ kPa})}{\left[(20 \text{ LPM}) \left(\frac{1 \text{ L}}{1000 \text{ m}^3} \right) \left(\frac{1 \text{ min}}{60 \text{ s}} \right) \right]^2} = \mathbf{0.090 \times 10^9 \frac{\text{kPa s}^2}{\text{m}^6}} \quad (44)$$

Using the obtained loss coefficient values and **Equation 39**, the overall pressure drop was calculated.

$$\begin{aligned}
 \Delta P &= (k_{MTR} + k_{MC} + k_{HX})Q_w^2 \\
 &= [(2.100 + 1.235 + 0.090)(10^9)] \left[(12 \text{ LPM}) \left(\frac{1 \text{ L}}{1000 \text{ m}^3} \right) \left(\frac{1 \text{ min}}{60 \text{ s}} \right) \right]^2 \quad (45) \\
 &= \mathbf{137 \text{ kPa}}
 \end{aligned}$$

From these calculations, it is apparent that a suitable pump must be able of delivering a flow rate of 12 LPM at a minimum of 137 kPa. Realistically, it must be capable of a relatively higher pressure to ensure that cavitation will not occur.

A 24V pump (GRI Int-G7060) was provided at no cost by Gorman Rupp Industries (GRI). Performance data provided by the manufacturer was used to create a performance curve for the pump. **Equation 45** was used to create a system resistance curve. These curves were plotted together, shown in **Figure 14**.

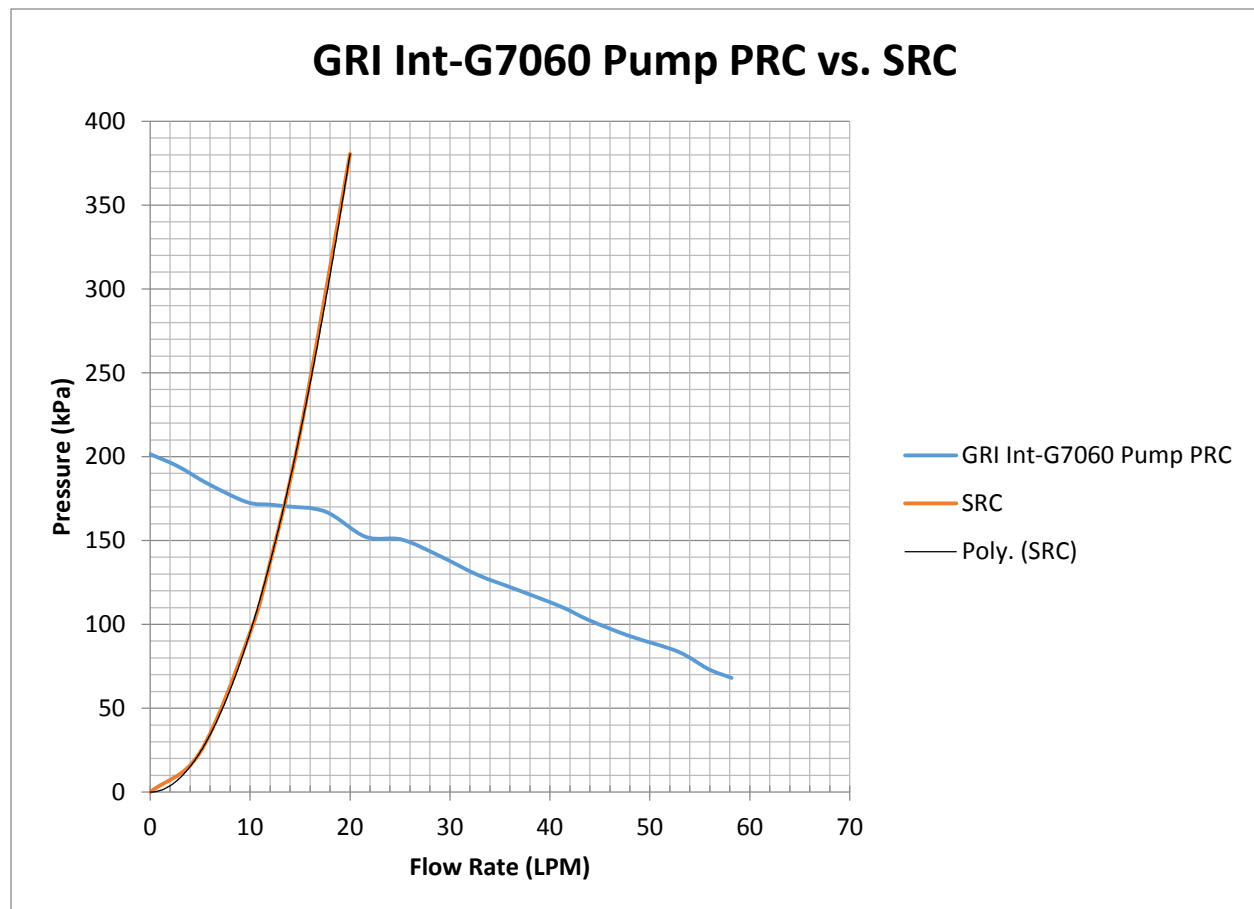


Figure 14: System Resistance Curve versus Pump Performance Curve

By analyzing **Figure 14**, it can be seen that the pump is capable of delivering more than enough pressure at a flow rate of 12 LPM. A more accurate estimate for this pressure was obtained by interpolating the

provided data. It was found that the pump is capable of delivering a flow rate of 12 LPM at 171.4 kPa and thus is suitable for this application.

Coolant Line Diameter Selection

It was necessary to decide an appropriate coolant line internal diameter for the system. This was a critical task due to the mix of inlet and outlet sizes throughout the system. Unfortunately, the pump inlet and outlet diameters are designed for a 1 inch inner diameter hose while the motor and motor controller inlets and outlets are designed for a 3/8 inch inner diameter hose. If a 1 inch ID is used, many unusual or custom fittings must be used to fit the hose to the motor and motor controller. However, a 3/8 inch ID hose has a significant pressure loss due to friction. Therefore, the pressure loss through the hose was determined for numerous inner diameter sizes. Based on the vehicle geometry, a hose length of 4 feet was used for calculations. The first step in this process was to determine the Reynolds number using **Equation 46**.

$$Re = \frac{QD}{\nu A} = \frac{QD}{\nu \frac{\pi}{4} D^2} = \frac{4Q}{\nu \pi D} \quad (46)$$

Note that D is the inner diameter of the hose, A is the area of the hose, and ν is the kinematic viscosity of the water. After determining the Reynolds number, the Moody friction factor, f , was determined using the following equation:

$$f = \frac{1.325}{\left[\ln \left(\frac{\epsilon}{3.7D} + \frac{5.74}{Re^{0.9}} \right) \right]^2} \quad (47)$$

where ϵ is the absolute roughness of the rubber tube and is equal to 0.0016 millimeters. The pressure loss due to friction in the hose could then be calculated using the following equation:

$$\Delta P_L = \rho \frac{V^2}{2} f \frac{L}{D} = \rho \left(\frac{8Q^2}{\pi^2 D^4} \right) f \frac{L}{D} \quad (48)$$

where L is the length of the hose and all other variables are consistent with previous definitions.

Equations 46, 47, and 48 were used to calculate the pressure loss for hoses with inner diameters of 3/8 inch, 1/2 inch, and 5/8 inch. These values are displayed in **Table 4**.

Pressure Loss Calculations			
	3/8"	1/2"	5/8"
<i>Re</i>	44153	33115	26492
<i>f</i>	0.0477	0.04	0.036
ΔP (kPa)	24.05	4.79	1.41

Table 4: Pressure loss calculations for various hose inner diameters

After performing these calculations, a hose with an inner diameter of 5/8 inch was selected due to its minimal pressure loss as well as the availability of the required reducers and couplers. Neglecting pressure drop across fittings, the total pressure loss in the system including in the hose is **138.41 kPa**. This is significantly lower than the pressure provided by the pump. Therefore, pressure at the pump inlet will be approximately 33 kPa and cavitation will not be an issue.

Miscellaneous Design Tasks

During the cooling system design process, other various parts needed to be designed. These are highlighted in the subsequent portions of this document.

Motor Coolant Fittings

Due to the size difference between the motor coolant fittings and the coolant hose, custom fittings were required for the motor coolant inlet and outlet. These fittings were designed to thread into existing tapped holes (12mm x 1.75) in the motor, fit within the preexisting motor brackets, and accept a hose with a 5/8 inch ID. To simplify the manufacturing process, aluminum weld-on barbs were purchased and welded to the custom fittings. The assembled fittings are displayed in **Figure 15** and **16**. The fittings in the drivetrain assembly are shown in **Figure 17**. Drawings for the manufactured portions of these fittings are available in the **Appendix**.

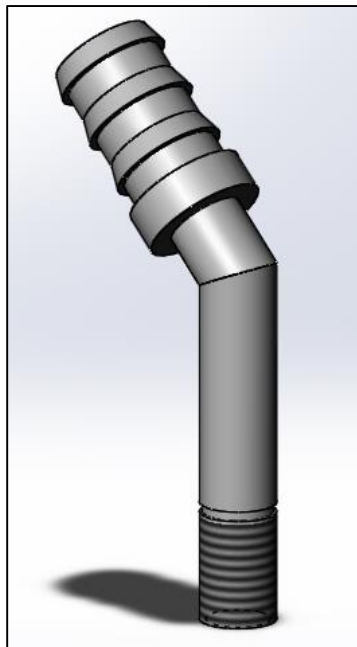


Figure 15: 45° Motor coolant fitting

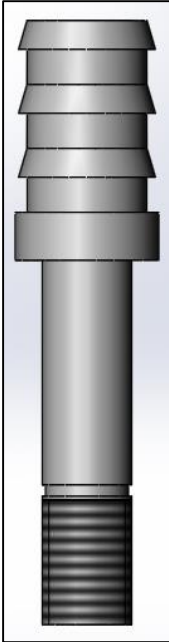


Figure 16: Straight motor coolant fitting

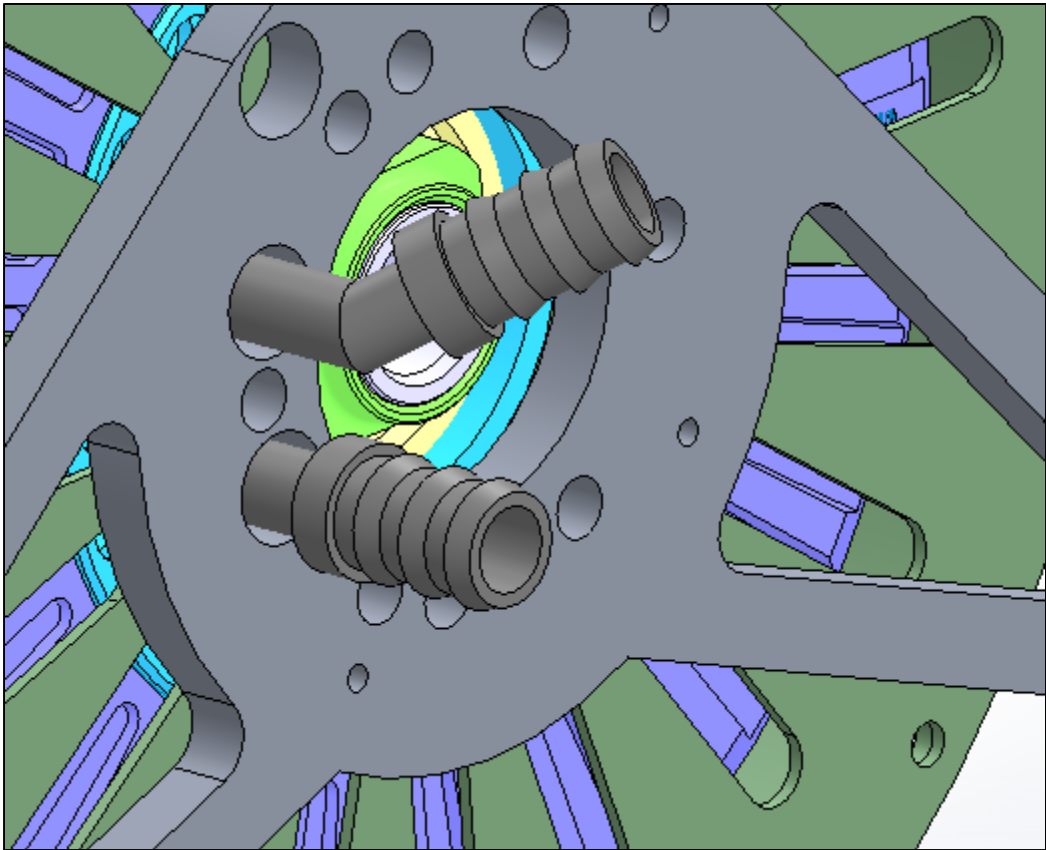


Figure 17: Motor coolant fittings in motor and motor brackets

Fan Mounts

Custom brackets were designed to fix the cooling fan to the radiator in a pulling configuration. One pair of each unique bracket design is used to attach the fan to the rear face of the radiator. By design, the outer aluminum brackets fit flush to the edge of the radiator and against a preexisting tab. These brackets are welded to each tank of the radiator. The two attachment brackets were designed with airflow in mind and feature thin support sections. These brackets bolt to the fan as well as the outer radiator bracket resulting in a sturdy but easily removable connection. The fan mounts are displayed in **Figure 18** and **19**. The fan and radiator assembly (hardware not shown) is displayed in **Figure 20**.



Figure 18: Outer radiator-fan attachment bracket

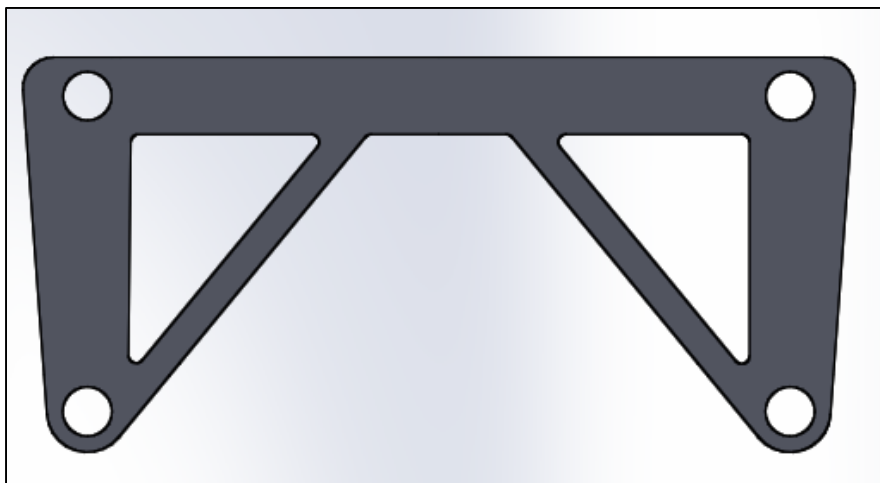


Figure 19: Radiator-fan attachment bracket

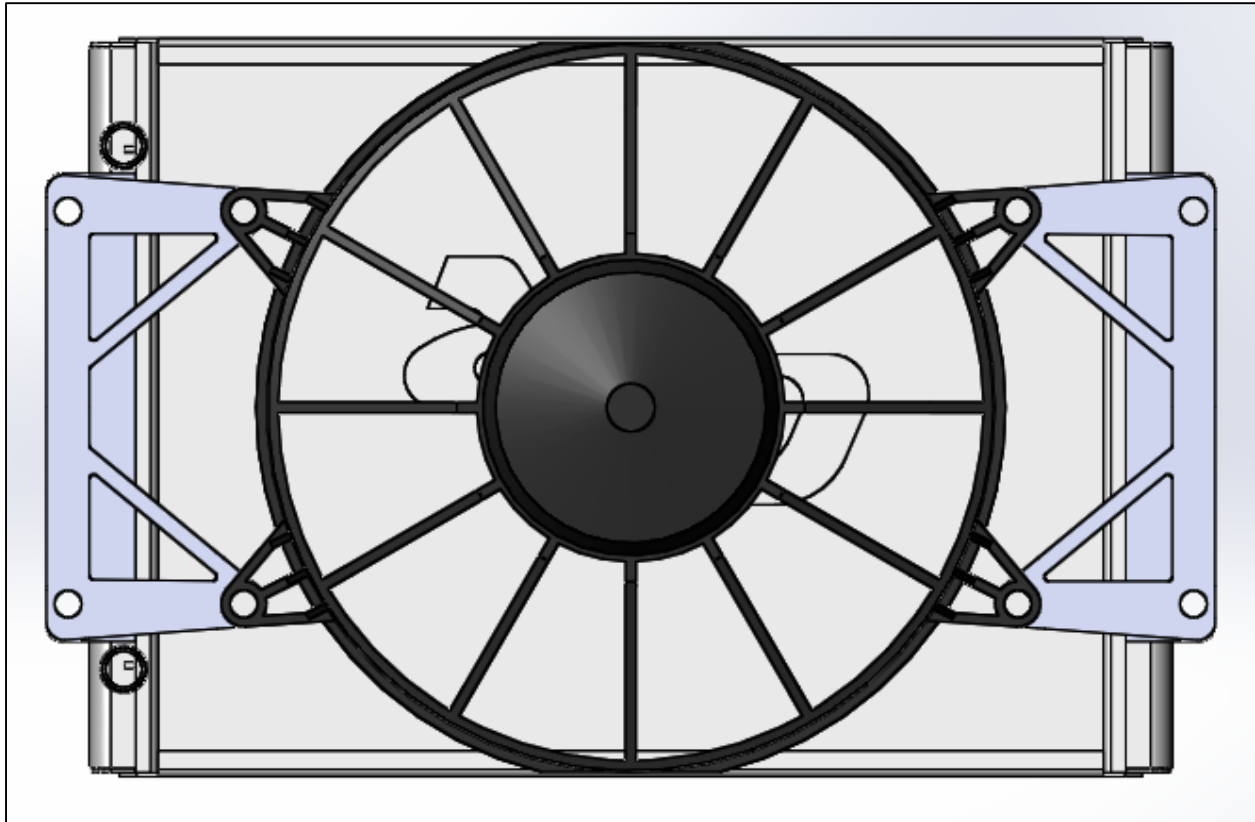


Figure 20: Radiator and fan attachment using attachment brackets

Duct Design

As a result of the geometry of the vehicle, possible placement areas for the radiator were quite limited. After extensively considering every possible position on the vehicle, it was decided that the best location that fit within the official FSAE rules was behind the driver and above the drivetrain assembly. The radiator was oriented at an angle to match the angle of the large structural frame members that support the roll hoop. Although this location is more than suitable for the radiator, it does not provide the best airflow to the radiator. Therefore, an inlet duct was designed to direct air to the radiator. It was determined that the optimal location for the duct inlet is above the driver's head within the roll hoop. This location provides an opening that is entirely unobstructed throughout the duration of the vehicle's operation for even the largest driver's body structure. Additionally, the location of the duct is primarily behind the driver's head and shoulders as well as the headrest assembly, thus decreasing the amount of drag created by the duct.

The duct features a divergent design for a few reasons. For one, a divergent design allows for a small opening that decreases the entrance ram air pressure. This allows air to enter the duct more easily than a larger opening. The divergent design also slows down the air velocity as it approaches the radiator face which causes the air to spend more time in the core of the radiator. Perhaps most importantly, the divergent design of the duct dramatically increases the static pressure of the air at the face of the radiator. This creates a large pressure differential across the radiator which ultimately forces air through the radiator's core. The inlet of the duct is displayed in **Figure 21**. The duct and radiator orientation are displayed in **Figure 22**.

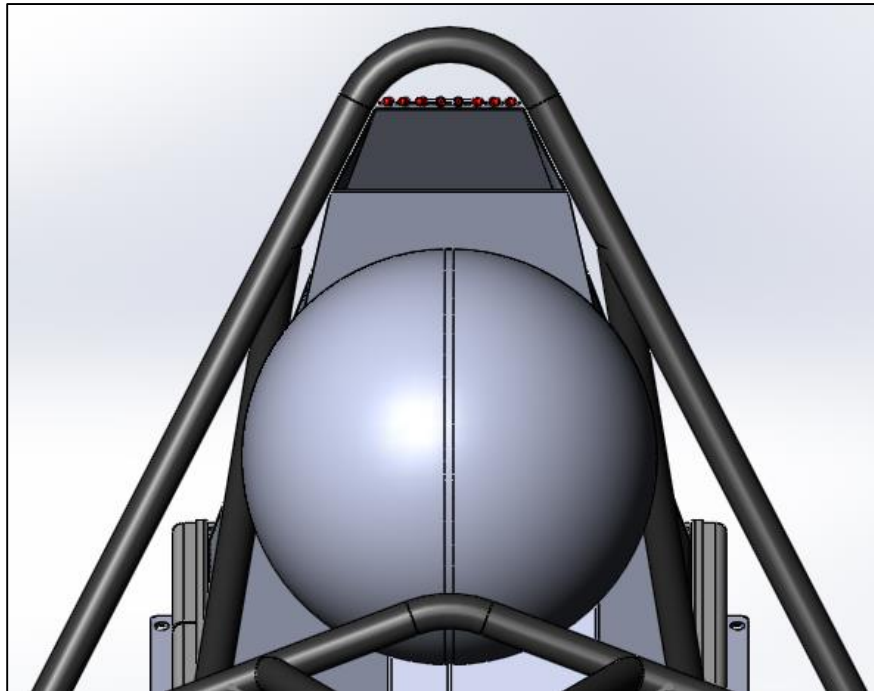


Figure 21: Radiator duct inlet area

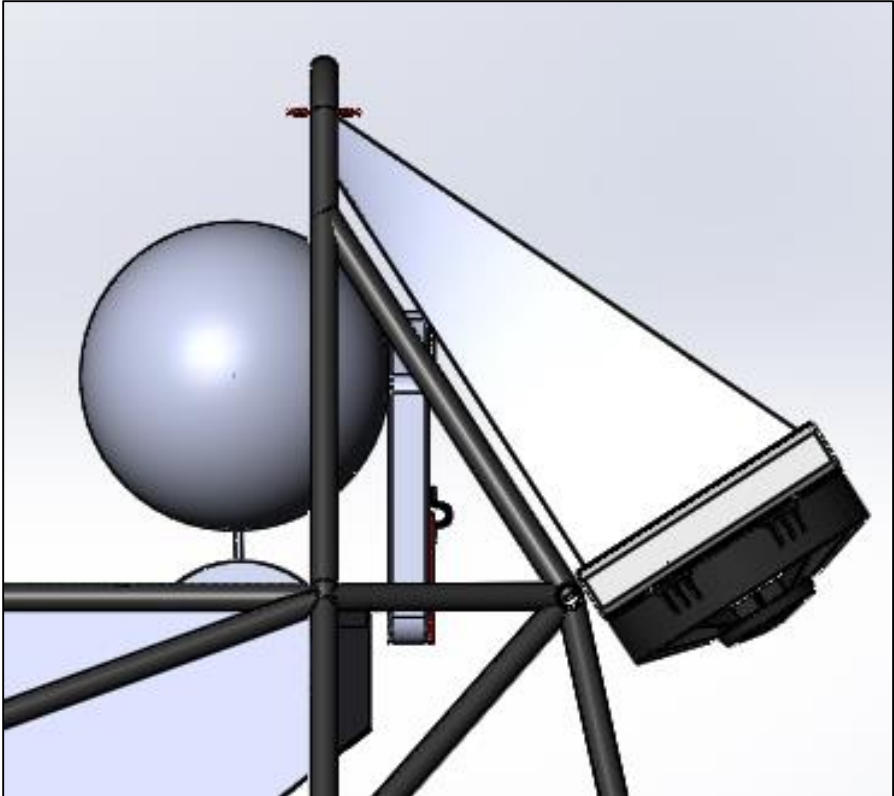


Figure 22: Radiator and duct orientation

Pump Mount

A mounting plate for the pump was designed in order to securely attach the pump to the frame. This plate was designed to allow for easy removal of the pump. The plate is attached to the frame by filling in a laser cut slot with a plug weld. This slot is in the center of the plate to allow all mounting hardware to clear the frame member and be exposed for easy access. The mounting plate is displayed in **Figure 23**.

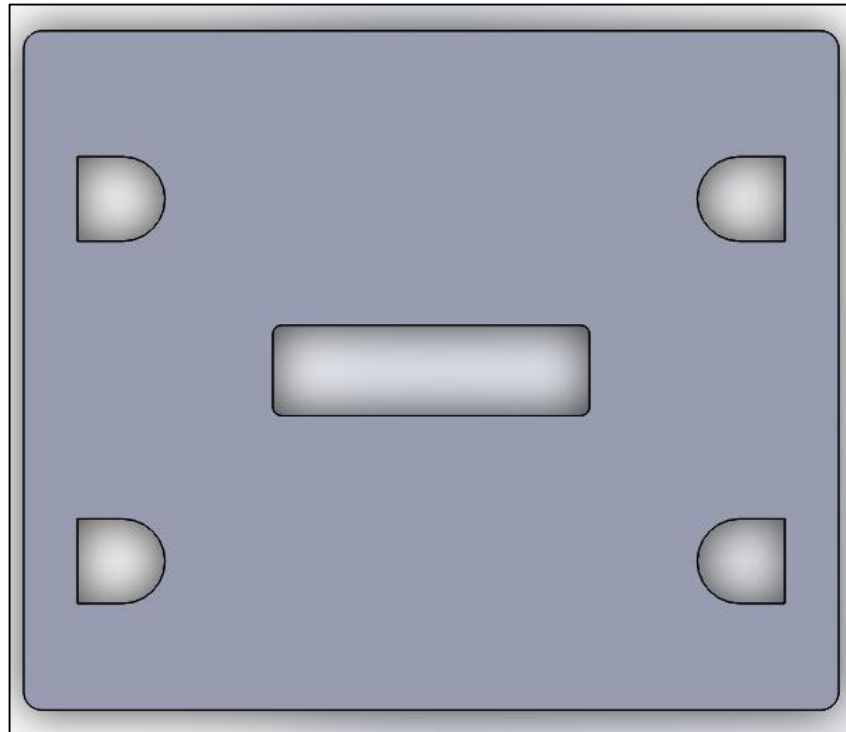


Figure 23: Pump mounting plate

Other Mounting Tabs

Various mounting tabs were created to attach the cooling system to the frame. Due to the simplistic nature of these tabs, the design process will not be covered in this document.

Manufacturing and Testing

At the time of the completion of this document, the manufacturing process is just beginning. There is a relatively limited amount of on-site manufacturing. All mounting tabs and brackets are being laser cut by a third party. The motor coolant fittings are being manufactured using a lathe, cold-cut saw, and a welder. Coolant line will be cut to size as deemed necessary.

Upon completion of all manufacturing, the vehicle will undergo strenuous testing before heading to competition. This testing will consist of various dynamic event simulations such as endurance, autocross, acceleration runs, and the skid pad event. In conjunction with the team's lead electrical engineer, temperature sensors will be used to evaluate the performance of the cooling system. This data will be used to determine if any minor changes are necessary.

Conclusion

The purpose of this design process was to research, design, and create an effective cooling system for an electric FSAE vehicle. The hope for this design is to not only be an effective and efficient system that guarantees the performance of the drivetrain components, but to serve as a guide for the electric vehicle's cooling system design for years to come. Although the real world performance of the cooling system will not be known until testing is complete, it is believed that this system will have no issues providing ample cooling for the drivetrain components of the vehicle.

Acknowledgements

This design project would not have been possible without the endless support and invaluable input of Dr. Richard Gross.

Additionally, the author would like to express his gratitude to The University of Akron FSAE Electric Vehicle Team's lead electrical engineer, Richard Johnson, for his efforts on this project.

Sources

Gross, R. Ph.D., 2015, Associate Professor Emeritus at The University of Akron, OH, private communication.

Hazen, E., "Cooling Systems 101 – An Overview of Cooling Systems and its Components," C&R Racing, Indianapolis, IN.

Kays, W. M. and London, A. L., 1984, Compact Heat Exchangers, McGraw-Hill Book Company, New York, NY.

Rinehart Motion Systems, LLC, 2012, "PM Family Data Sheet," RMS, Wilsonville, OR.

[1] Speedway Motors, 2014, "The Difference Between Down-Flow and Cross-Flow Radiators," from <http://www.speedwaymotors.com/Tech/cooling-aluminum-radiators-downflow-vs-crossflow.html>

[2] Gross, R. Ph.D., 2015, "Chapter 11 – Cooling System Design," Unpublished, Akron, OH.

[3] OptimumG, 2012, "OptimumLap," from <http://www.optimumg.com/software/optimumlap/>

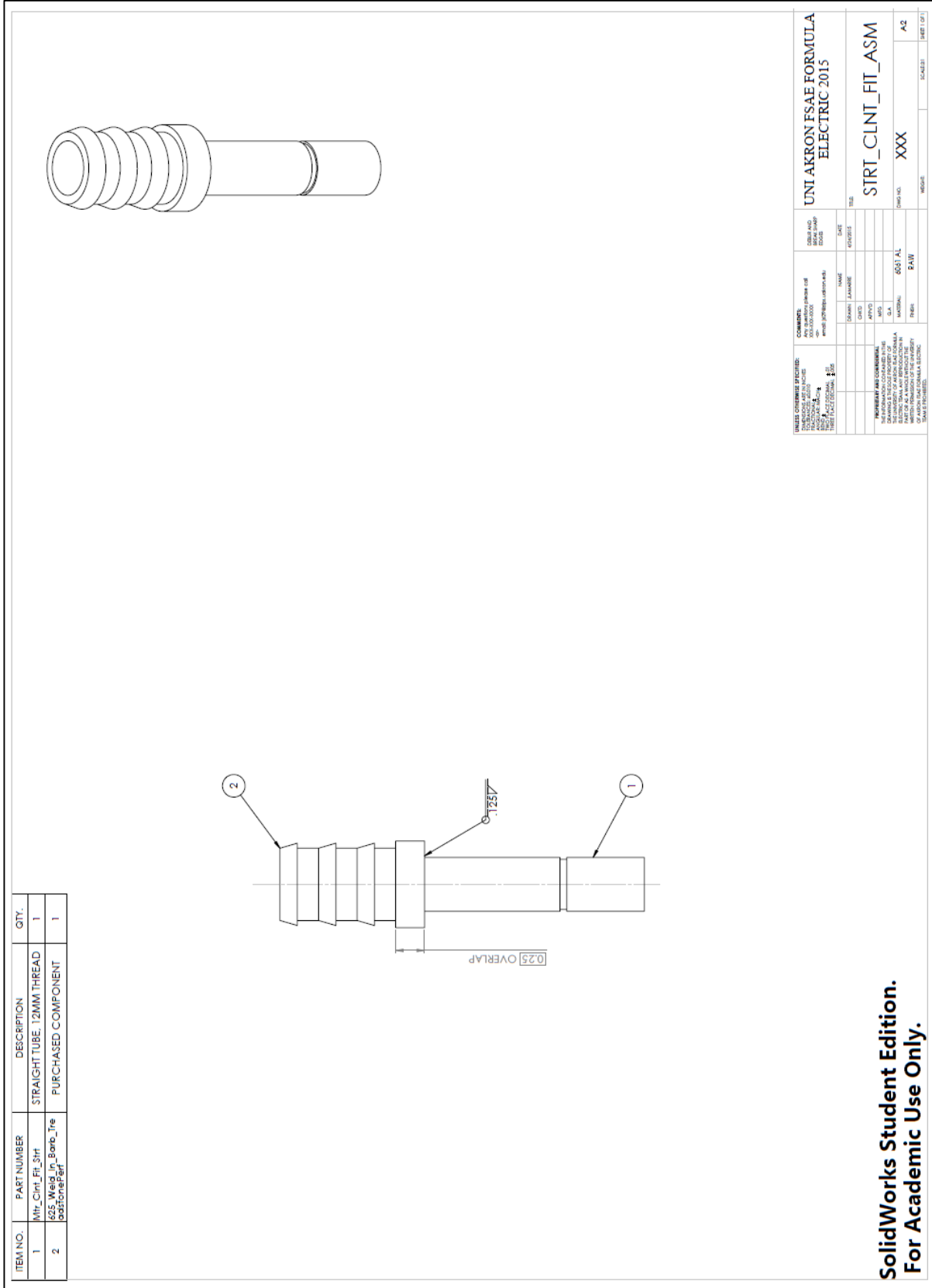
[4] OptimumG, 2012, "OptimumLap Track Database," from <http://share.optimumg.com/tracks/>

[5] ENSTROJ, 2014, "Manual for EMRAX motors," ENSTROJ, Slovenia, Europe.

[6] SPAL AUTOMOTIVE, 2015, "Axial Fans – 24V, VA15-BP70/LL-39A Product Features," from http://www.spalautomotive.com/eng/products/view_axial.aspx?id=VA15-BP70_LL-39A

[7] ENSTROJ, 2014, "Emrax Liquid Cooling Flow Rates," ENSTROJ, Slovenia, Europe.

[8] Brune, C., 2012, "Pressure Drop Test," Revision-02, RMS, Wilsonville, OR.



**SolidWorks Student Edition.
 For Academic Use Only.**

Drawing 2: Straight motor coolant fitting assembly

